

Effects of operating conditions on flow and heat transfer characteristics of mist cooling in a square ribbed channel[†]

Tieyu Gao¹, Junxiong Zeng¹, Qingfeng Xia^{2*}, Jun Li¹ and Jianying Gong¹
¹School of Energy and Power Engineering, Xi'an Jiaotong University, Xi'an, 710049, Shaanxi, China

²Onsey Thermo-fluids Lab, Department of Engineering Science, University of Oxford, Parks Road, Oxford OX1 3PJ, United Kingdom

(Manuscript Received 000 0, 2009; Revised 000 0, 2009; Accepted 000 0, 2009) -please leave blank

Abstract

Flow and heat transfer characteristics of mist/steam cooling and mist/air cooling in a square channel with 60° rib angle are numerically investigated for a wide range of operating parameters, such as Reynolds number ranging from 10,000 to 60,000, reference pressure from 0.1MPa to 0.5MPa and inlet temperature from 120 °C to 200 °C. Also, the heat transfer characteristics of mist cooling are compared with the corresponding experiment of cases of single-phase coolant such as steam and air. The 3D steady Reynolds-averaged Navier–Stokes equations with a standard $k-\omega$ (insert symbol instead of figure in abstract) turbulent model are solved by using commercial software ANSYS CFX. The CFD model has been validated by experimental data for steam-only case with a good agreement. In addition, distribution and evolution of secondary flow in the ribbed channel are analyzed by vortex core technology and their effects on heat transfer are investigated for these four coolants. The results show that the strength of longitudinal secondary flow has a great significant influence on the Nusselt number (Nu) distribution on the ribbed surface. The Nu Nusselt number distribution is values are periodically distributed in stream-wise direction for steam and air cooling, whereas these are Nusselt number gradually increased-increases along the same direction for mist/steam and mist/air cooling. The parameter study suggests that heat transfer characteristics of mist cooling are insensitive to pressure, but inversely correlated with coolant inlet temperature compared with steam and air cooling.

Keywords: Numerical simulation; Mist cooling; Ribbed channel; Heat transfer; Vortex core.

1. Introduction

Gas turbine has been widely employed in land-based power generation, marine and aerospace propulsion, etc. Increasing turbine inlet temperature (TIT) is one of the major approaches to improve the thermal efficiency of gas turbines. However, TIT about 2000K for advanced gas turbines about 2000K has been attempted, which is far beyond the melting point of metal material for gas turbine blades and vanes. Consequently, advanced cooling technologies are indispensable to protect gas turbine blades and vanes from high temperature corrosion and creeping damage in high-performance gas turbines. In addition to thermal barrier coating and film cooling, internal cooling for gas turbine is the common approach to reduce the heat load on blades and vanes. Internal cooling can be categorized by coolant into traditional air cooling, closed-loop steam cooling and two-phase flow closed-loop mist/steam or mist/air cooling.

Various kinds of rib (turbulence generator) in serpentine passages can enhance the heat transfer between the coolant and hot surface of gas turbine blades. Internal cooling can be categorized by coolant into traditional air cooling, closed-loop

steam cooling and two-phase flow closed-loop mist/steam or mist/air cooling.

Since the 1980s, Han et al. [1–3] and Park et al. [4] have experimentally and systematically investigated the heat transfer and friction characteristics of air cooling in rectangular channels with five aspect ratios ($W/H=1/4, 1/2, 1/1, 2/1$ and $4/1$), four rib angles ($\alpha=30^\circ, 45^\circ, 60^\circ$ and 90°), two rib pitch-to-height ratios ($p/e=10$ and 20), respectively. Thereby, semi-empirical correlations corresponding to cooling performance to aspect ratio (W/H), rib angles (α), rib height (d) and Reynolds numbers (Re) were established in their studies. However, air cooling can not address the challenge of high TIT for advanced gas turbines because of its inferior heat transfer capacity.

Besides the established air cooling technology, steam with a higher specific heat capacity but a lower thermal conductivity than air has been widely studied for gas turbine internal cooling. Closed-loop steam cooling scheme can increase the thermal efficiency and power output of gas turbines in a combined cycle system via higher TIT and effectively-reduced air extraction from compressor. Gong et al. [5, 6], Liu et al. [7, 8] and Shi et al. [9] experimentally studied the heat transfer

[†] This paper was recommended for publication in revised form by Associate Editor 000 000 -please leave blank.

*Corresponding author. Tel.: +44 (0) 1865288733, Fax.: +44 (0) 1865288756

E-mail address: Qingfeng.xia@eng.ox.ac.uk

© KSME & Springer 2010

characteristics of steam coolant in rectangular ribbed channels with aspect ratios $W/H=1/4$, $1/2$, $1/1$ and rib angles $\alpha=30^\circ$, 45° , 60° and 90° . Their results indicated that the average Nusselt number in steam cooling ribbed channels was about 15% to 30% higher than that of air. In addition to geometric parameters for ribbed channels such as aspect ratio, rib angle and block ratio of rectangular channels, operating parameters such as inlet Reynolds number, operating pressure, temperature of steam coolant, and heat flux of ribbed surface are investigated for and heat flux of ribbed surface determine the flow and heat transfer behaviors of steam coolant. Some researchers also investigated the effects of operating conditions on flow and heat transfer characteristics of steam cooling in a rectangular ribbed channel. For example, Gao et al. [10] experimentally investigated the effects of inlet Reynolds number (Re) ranging from 30,000 to 140,000, inlet pressure ranging from 0.2MPa to 0.5MPa, heat flux of the ribbed surface ranging from 5 kW/m^2 to 20 kW/m^2 and superheat of steam coolant ranging from 13°C to 51°C on heat transfer characteristics of steam in a square channel with rib angle $\alpha=60^\circ$. The results demonstrated that the heat transfer coefficient increased increases rapidly with Reynolds number, but the inlet pressure, superheat of steam coolant and the heat flux of ribbed wall has have insignificant influence on heat transfer coefficient. This might be explained by the fact that the variation of Prandtl number within the laboratory operating conditions is minimal. Subsequently, Shui et al. [11] numerically studied study the effects of elevated operating conditions as in the working gas turbine, i.e., high pressure, high temperature and high Reynolds numbers on the thermal performance of steam coolant. The results suggest indicated that medium pressure of 3MPa to 4MPa, with a relatively lower Reynolds number of 30,000 and a lower temperature of 300°C obtained obtains the best thermal performance of steam within the elevated operating conditions.

Although, closed-loop steam cooling has the potential of better thermal performance than air cooling, one of the disadvantages is steam consumption [12, 13]. In order to replace air film cooling, the heat transfer coefficient of coolant has to be significantly enhanced (up to about $8000\text{--}10000\text{ W/m}^2\text{K}$). Extracting a large volume of steam from steam turbines leads to the decreased thermal efficiency of the steam turbines. Therefore, it is imperative to develop new advanced cooling technologies to address the above issues. One of the promising approaches to greatly enhance the heat transfer is to inject a small amount of mist into the steam or air flow. Due to the latent heat of evaporation, a lower temperature near the boundary layer is expected and an increased turbulence mixing caused by gas-droplet interactions may significantly boost the heat transfer performance. In the 2000s, Guo et al. [14–16] have conducted the first experimental investigation of mist/steam cooling heat transfer characteristics in a horizontal smooth tube and in a 180° bend tube. The results indicated that an averaged heat transfer enhancement of 50%–100% was obtained with 1%–3% mist injection is obtained from experi-

mental study, and a local heat transfer 200%–300% and 500% enhancement of local heat transfer 200%–300% and 500% was achieved for the horizontal tube and the 180° bend tube, respectively. Durmuş et al. [29] experimentally studied the heat transfer characteristics and pressure loss of concentric double pipe heat exchanger with a snail type swirl generator mounted at inlet of inner pipe. Also, the secondary flows (swirl flow patterns) in the pipe were visualized and discussed in their experiment. Ozgen et al. [30] experimentally investigated the energy efficiency of three types of double-flow flat-plate solar air heater, and suggest that the type I obtains the highest efficiency. This section is put forward, so the reference number needs adjustment.

Theoretically, it is encouraging for applying mist cooling to both gas turbine vane and blade under elevated operating conditions; and the performance of mist cooling has been moderately investigated. Wang et al. [17, 18] explored explore the feasibility of applying mist cooling to gas turbine vanes and blades by numerical simulation method. The results demonstrated that theoretically, it was encouraging for applying mist cooling to both gas turbine vane and blade under elevated operating conditions. Dhanasekaran et al. [19, 20] validated the numerical results of mist/steam cooling with the experimental data in a horizontal smooth tube and in a 180° bend tube respectively; the predicted results deviated 8% for steam-only and 16% deviation for mist/steam. A numerical study was performed by Dhanasekaran et al. [21] to investigate the heat transfer coefficient of mist/air in two-pass 45° ribbed channel with and without rotation. The results showed that the averaged heat transfer coefficient on leading edge and trailing edge for 45° ribbed rotational channel was increased 20% and 30% by injecting 2% mist, respectively. Elwekeel et al. [22], Liao et al. [23] and Zhang et al. [24] numerically studied the heat transfer performance of four kinds of coolants in 90° ribbed channel, in a wedge duct with pin-fins and in a two-pass ribbed channel with or without rotation, respectively. Their results indicated that mist/steam obtained the best thermal performance among all the coolants. Additionally, the thermal performance of various rib configurations including square rib, triangular rib and trapezoidal rib in mist/steam and mist/air cooling (6% mist) channel with 90° rib angle was compared by Elwekeel et al. [25, 26] using numerical scheme.

According to the research by Han [1], the secondary flow induced by flow separation on the leading edge of the inclined ribs was is the main cause for heat transfer enhancement. The evolution of the secondary flow in ribbed channels had has a significant influence on the heat transfer coefficient. Gao et al. [27, 28] have analyzed the vortices structure (the secondary flow distribution) in single-pass channel and two-pass channel with an aspect ratio $W/H=1/1$, rib angle $\alpha=45^\circ$, and the effects of these secondary flows on heat transfer were also is examined by employing vortex core visualization technology. The results demonstrated that the strong secondary flow regions achieved a relatively higher Nu distribution than others is found in regions with strong secondary flow.

Formatted: Font color: Auto, Highlight

Formatted: Font color: Auto

Formatted: Font color: Auto, Highlight

Durmuş et al. [29] experimentally studied the heat transfer characteristics and pressure loss of concentric double pipe heat exchanger with a snail type swirl generator mounted at inlet of inner pipe. Also, the secondary flows (swirl flow patterns) in the pipe were visualized and discussed in their experiment. Ozgen et al. [30] experimentally investigated the energy efficiency of three types of double flow flat plate solar air heater. Results showed that the type I obtained the highest efficiency. Recently, Gao et al. [31] also have investigated the distribution of secondary flows in a steam and air cooling ribbed channel with large aspect ratio ($W/H=4$) and revealed the relationships between these secondary flows and heat transfer enhancement. The results showed that it is found that steam and air had variation of coolant has little insignificant impact on the morphology of secondary flows, while the generation, separation and mixing of secondary flows can significantly improve the local heat transfer enhancement. I will not present this paragraph, it is not important and it will only reduce your contribution/innovation, just delete this paragraphs, the last sentence can be put into vortex structure analysis section.

Limited studies have been carried out on the effects of operating conditions on flow and heat transfer characteristics of mist/steam and mist/air cooling. Previous studies conducted by Gao et al. [10] and Shui et al. [11] mainly focused on the effects of operating conditions on heat transfer characteristics of steam cooling. Due to the evaporation mechanism of water droplets, the mist/steam and mist/air cooling enhancement performance can be more sensitive to operating conditions than single-phase coolant like steam or air. Therefore, the objective of this study is to numerically investigate the effects impact of operating conditions such as inlet Reynolds number, pressure and temperature on flow and heat transfer characteristics of mist/steam and mist/air cooling in a square channel with rib angle $\alpha = 60^\circ$. The heat transfer characteristics of mist/steam and mist/air are compared with steam and air under the identical operational conditions in this study. Additionally, the morphology and distribution of secondary flows in the ribbed channel with four kinds of coolants and the interaction between secondary flows and water droplets as well as its effects on heat transfer are also analyzed by vortex core technology.

2. Computational model and numerical method

2.1 Geometric configuration

In order to validate the numerical model against experimental data, the geometry of cooling channel adopted in the current study is the identical as Ref. [10]. Fig. 1 shows the schematic diagram of geometric model and the computational domain, consisting of which contains an extended entrance section, a ribbed duct and an extended outlet section. In order to guarantee improve model fidelity, the extended entrance section is incorporated to obtain a steady and fully developed flow situation inlet flow and the extended outlet section is to

avoid backflow. The ribbed duct is considered as the heated section. The detailed geometric parameters of computational domain, which are also adopted from Ref. [10], are shown in Table 1, which are also adopted from Ref. [10].

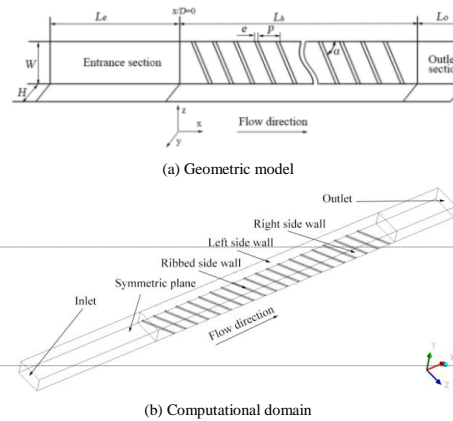


Fig. 1. Schematic diagram of (a) geometric model and (b) computational domain

Table 1. Parameters of computational model

Parameter	Value	Parameter	Value
$W \times H$	40×40	p/e	10
e (mm)	1.9	α ($^\circ$)	60
D (mm)	40	L_e (mm)	200
e/D	0.0475	L_d (mm)	400
p (mm)	19	L_o (mm)	100

2.2 Parameter definition

The Reynolds number (Re) for the cooling channel is defined as:

$$Re = \rho u D / \mu \quad (12)$$

where D is the hydraulic diameter of the channel, and μ is dynamic viscosity of coolant.

The local Nusselt number (Nu) is written as:

$$Nu = hD / \lambda = [q / (T_w - T_b)] (D / \lambda) \quad (13)$$

where q is the heat flux of the heated walls; T_w is the temperature of the ribbed side wall; T_b is the bulk temperature at x -direction; λ is the thermal conductivity of fluid coolant.

According to Dittus-Boelter correlation, the Nusselt number (Nu_o) for the fully developed turbulent flow in a smooth tube is defined as:

$$Nu_o = 0.023 Re^{0.8} Pr^{0.4} \quad (14)$$

The friction factor for fully developed flow in a smooth tube is expressed as:

$$f_o = 0.079 Re^{-0.25} \quad (15)$$

I adjust these two friction factor, to be more logical. Meanwhile, The Fanning friction factor in the ribbed channel is defined as:

Formatted: Highlight

Formatted: Highlight

Formatted: Highlight

Formatted: Highlight

$$f = \Delta PD / (2\rho \Delta Lu^2) \quad (15)$$

In order to evaluate the balanced cooling performance and pressure loss characteristics, the friction factor for fully developed flow in a smooth tube is expressed as

$$f_o = 0.079 Re^{-0.25} \quad (16)$$

The thermal performance factor (η) is defined in the current study as:

$$\eta = (Nu / Nu_o) / (f / f_o)^{1/3} \quad (17)$$

2.2.3 Numerical method

In the present study, the Eulerian-Lagrangian particle tracking method is applied to investigate the heat transfer characteristics of mist/steam and mist/air cooling in a square ribbed channel. To simulate the mist/steam (or mist/air) cooling, the mist/steam (or mist/air) coolant mainly consists of water droplets (mist) and a variable composition mixture contained by steam (or air) and water vapor. Since the volume fraction of the mist over steam (or air) flow is small in this study, the water droplets and steam (or air) are considered as discrete phase and continuous phase, respectively. The trajectories of discrete phase are calculated by the Lagrangian method, while the continuous phase is formulated with the Eulerian method in ANSYS CFX solver. Furthermore, the fully coupling is selected to simulate the mutual effects between the continuous phase and the discrete phase flow. The fully coupling is selected in ANSYS CFX solver to simulate the mutual effects between the continuous phase and the discrete phase flow. The impact of the droplets on the continuous phase is considered as source terms to the steady-state governing equations of mass, momentum and energy. [ref to Ansys manual]. The time-averaged steady governing equations for both continuous phase and discrete phase are given below:

2.2.1 Continuous phase

Mass equation

$$\frac{\partial}{\partial x_i} (\rho u_i) = S_m \quad (1)$$

Momentum equation

$$\frac{\partial}{\partial x_i} (\rho u_i u_j) = \rho g_j - \frac{\partial p}{\partial x_j} + \frac{\partial}{\partial x_i} (\tau_{ij} - \rho \overline{u_i u_j}) + F_j \quad (2)$$

Energy equation

$$\frac{\partial}{\partial x_i} (\rho c_p u_i T) = \frac{\partial}{\partial x_i} (\lambda \frac{\partial T}{\partial x_i} - \rho c_p \overline{u_i T}) + \mu \Phi + S_h \quad (3)$$

Species transport equation

$$\frac{\partial}{\partial x_i} (\rho u_i C_j) = \frac{\partial}{\partial x_i} (\rho D_j \frac{\partial C_j}{\partial x_i} - \rho \overline{u_i C_j}) + S_j \quad (4)$$

where the source terms (S_m , F_j , S_h) represent the contributions including the mass and heat transfer from the discrete phase to the continuous phase in the process of water droplets evaporation. τ_{ij} is viscous shear stress tensor. λ and $\mu \Phi$ represent the thermal conductivity and viscous dissipation, respectively. D_j and C_j are the diffusion coefficient and mass

ratio of species j , respectively. $-S_j$ is the source term of this species. It should be noted that the species transport equation only occurs in the simulation of mist/air cooling because the mist/air coolant is a two-component two-phase flow different from the mist/steam coolant, which is a one-component two-phase flow where the steam is the only main flow.

2.2.2 Discrete phase

The motion equation of the water droplets is written as:

$$m_p \frac{du_p}{dt} = \Sigma F \quad (5)$$

where ΣF represents the combined force acting on the water droplets, which mainly contains the drag force, buoyancy force caused by gravity, virtual (or added) mass force and pressure gradient force. The detailed description of the combined force can be found in Ref. [32].

The heat transfer of water droplets is given by the following equation.

$$m_p c_p \frac{dT_p}{dt} = \pi d_p \lambda Nu (T - T_p) + \frac{dm_p}{dt} h_{fg} \quad (6)$$

The temperature rate of change of temperature of water droplets is determined by convective heat transfer (the first part of right hand side of Eq. (6)) and latent heat for evaporation transfer coupled with mass transfer (see the second part of right hand side of Eq. (6)). m_p is the droplet mass and c_p is the specific heat of droplets. T and T_p are the temperature of continuous phase and mist, respectively. d_p is the diameter of droplets and λ is the thermal conductivity of continuous phase. dm_p/dt is the rate of evaporation and h_{fg} is the latent heat of droplets. Nusselt number is given by:

$$Nu = 2 + 0.6 Re^{0.5} Pr^{0.33} \quad (7)$$

The liquid evaporation model with heat and mass transfer adopted in ANSYS CFX 14.0 solver uses two mass transfer correlations depending on whether the droplet is above or below the boiling point. The boiling point of droplets is determined governed by Antoine equation given by:

$$\log_{10} P_{sat} = A - \frac{B}{T + C - 273.15} \quad (8)$$

where, A, B and C are constant coefficients.

When the particle is above the boiling point, droplet the rate of mass transfer is determined by the convective heat transfer:

$$\frac{dm_p}{dt} = - \frac{\pi d_p \lambda Nu (T - T_p)}{h_{fg}} \quad (9)$$

When the particle droplet is below the boiling point, the rate of mass transfer is given by the following equation:

$$\frac{dm_p}{dt} = \pi d_p \rho_v D_v Sh \frac{W_v}{W} \log \left(\frac{1 - X_p}{1 - X} \right) \quad (10)$$

where ρ_v , D_v is the dynamic diffusivity of vapor, W_v and W represent the molecular weights of the vapor and the mixture in the continuous phase respectively. X_p and X are the mole fractions of the evaporating component at the droplet surface and in the gas phase, respectively. Sh is the Sherwood number given by:

Formatted: Font color: Blue

$$Sh = 2 + 0.6Re^{0.5} \left(\frac{\mu}{\rho_v D_v} \right)^{1/3} \quad (11)$$

2.3 Parameter definition

The Reynolds number (Re) is defined as

$$Re = \rho u D / \mu \quad (12)$$

where D is the hydraulic diameter of the channel, and μ is dynamic viscosity of coolant.

The local Nusselt number (Nu) is written as:

$$Nu = hD / \lambda = [q / (T_w - T_b)] (D / \lambda) \quad (13)$$

where q is the heat flux of the heated walls; T_w is the temperature of the ribbed side wall; T_b is the bulk temperature at x -direction; λ is the thermal conductivity of fluid coolant.

According to Dittus-Boelter correlation, the Nusselt number (Nu_o) for fully developed turbulent flow in a smooth tube is defined as

$$Nu_o = 0.023 Re^{0.8} Pr^{0.4} \quad (14)$$

The Fanning friction factor in the ribbed channel is defined as

$$f = \Delta P D / (2 \rho A u^2) \quad (15)$$

The friction factor for fully developed flow in a smooth tube is expressed as

$$f_o = 0.079 Re^{-0.25} \quad (16)$$

The thermal performance factor (η) is defined as:

$$\eta = (Nu / Nu_o) / (f / f_o)^{1/3} \quad (17)$$

2.4 Boundary conditions

The mass flow rate is assigned to the inlet according to corresponding Reynolds number ranging from 10,000 to 60,000. A turbulence intensity of 5% is applied to inlet. This study aims to investigate the effects of operating conditions including the coolant temperature and pressure on heat transfer characteristics of both mist/steam and mist/air cooling. Thus, the inlet temperature of steam and air ranging from 120°C to 200°C and the reference pressure of computational domain from 0.1MPa to 0.5MPa are considered studied in the current study, while the heat flux of the ribbed surface and the two sides of smooth surfaces are kept at a constant value of 10,000 W/m². The other walls including the entrance section and the outlet section are considered as adiabatic to model wall with thermal insulation in the experimental setup. All the walls of the channels are specified as no slip boundary condition. Due to the symmetry of this geometric model with respect to positive y-direction (see Fig. 1), a symmetry condition is specified at the symmetric plane. 这一段的问题在于句子之间没有逻辑，东一句，西一句 The mass flow rate is assigned to the inlet according to corresponding Reynolds number ranging from 10,000 to 60,000. A turbulence intensity of 5% is applied to inlet. All the walls of the channels are specified as no slip boundary condition.

For the discrete phase, a uniform distribution of water droplets is allocated at inlet with an average diameter of 10 μm for both mist/steam and mist/air cooling. The mass ratio of mist over steam and/or air flow is 2%. For the droplet wall bounda-

ry condition, Dhanasekaran et al. [20] confirmed that the reflect boundary condition is better than wall film boundary condition for predicting heat transfer enhancement of mist/steam in their simulations. Additionally, Refs. [21–24] also employ have directly used the reflect boundary condition to simulate the flow and heat transfer behaviors of mist/steam or mist/air. Hence Thereby, the reflect boundary condition is also adopted in this study to calculate the trajectories of droplets, which means that the droplets will elastically rebound off once reaching the wall. The detailed description of wall droplet boundary condition can be found in Refs. [17, 20] and is not repeated here.

2.5 Grid sensitivity study

The commercial software ANSYS CFX 14.0 has been used in the current study to investigate the effects of operating conditions on flow and heat transfer characteristics of mist/steam and mist/air cooling in a square ribbed channel. The convective term and turbulence terms are solved with high resolution discrete scheme. The root mean square residual of continuity and momentum equations is less than 10⁻⁵ and that of energy as well as turbulent kinetic energy is less than 10⁻⁴. Furthermore, the area averaged temperature on the ribbed surface is monitored to confirm that the convergence has been achieved.

Fig. 2 shows the local details of structured meshes generated by ANSYS ICEM CFD for the fully developed region of computational domain. The cells in near wall region have been refined to guarantee $y^+ < 1$ as requested by automatic wall function in ANSYS CFX 14.0 steady solver.

A grid sensitivity study has been performed using $k-\omega$ turbulence model at $Re=58585$ with the mesh numbers ranging from 2.23 million to 6.06 million. The effect of mesh numbers on Nusselt number distribution along the centerline of the bottom surface with rib is shown in Fig. 3. It can be seen that when mesh numbers exceed 3.23 million, Nusselt number distribution is independent on mesh density. In order to guarantee the computational accuracy, the final mesh size of about 5.32 million is adopted in this study.

The convective term and turbulence terms are solved with high resolution discrete scheme. The root mean square residual of continuity and momentum equations is less than 10⁻⁵ and that of energy as well as turbulent kinetic energy is less than 10⁻⁴. Furthermore, the area averaged temperature on the ribbed surface is monitored to confirm that the convergence has been achieved. 这一段不重要 应该删去

Formatted: Highlight

Formatted: Highlight

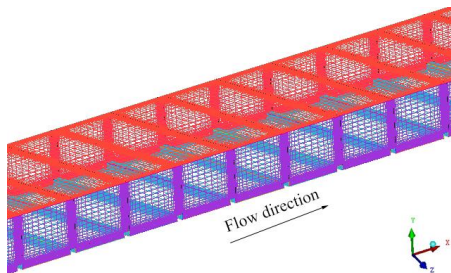


Fig. 2. Computational mesh details

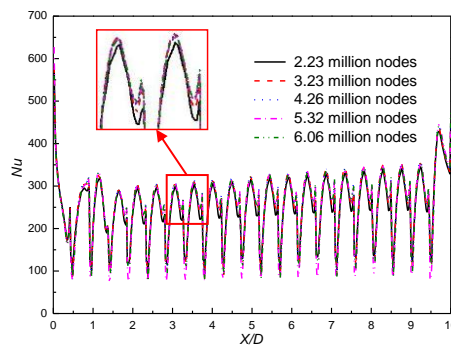


Fig. 3. Grid sensitivity study

2.6 Validation of numerical method

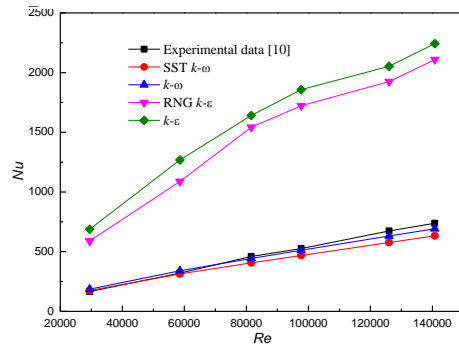
Due to lack of experimental study on mist/steam and mist/air cooling for gas turbine internal ribbed channels in open literature, the CFD procedure and methodology adopted in the current study follow those in the numerical investigations of Refs. [21–26]. Furthermore, this numerical model is validated with experimental data for air-only case with the same boundary conditions. In this study, the boundary conditions are also modelled from the experimental study [10]. Four turbulence models including the SST $k-\omega$, standard $k-\omega$, RNG $k-\epsilon$ and standard $k-\epsilon$ are compared in the current study. Due to lack of experimental study on mist/steam and mist/air cooling for gas turbine internal ribbed channels in open literature, the CFD procedure and methodology adopted in the current study follow those in the numerical investigations of Refs. [21–26], which were validated with experimental data for air-only. Fig. 4 shows the area-averaged Nusselt number of the ribbed wall varying with Reynolds number for different turbulence models. It can be concluded that the turbulence models of RNG $k-\epsilon$ and standard $k-\epsilon$ greatly over-predict the Nusselt number, while the numerical results of SST $k-\omega$, standard $k-\omega$ models are fairly consistent with experimental data in the low Reynolds number range ($Re < 60,000$) for the wall bounded internal

flow. However, the numerical results of both SST $k-\omega$ and standard $k-\omega$ models are slightly under-predicted the Nusselt number for high Reynolds number ($Re > 80,000$) compared with experimental data and the trend of this under-prediction gradually increases with Reynolds number.

Comparatively, the prediction of standard $k-\omega$ model is preferred to SST $k-\omega$. For example, the predicted values of standard $k-\omega$ model have an average deviation of -6.3% at $Re = 14,000$, while the deviation for SST $k-\omega$ is -14.3% under the identical conditions. Fig. 5 plots the comparison of numerical results of SST $k-\omega$ and standard $k-\omega$ models with the experimental correlation for Reynolds number less than 60000 which is given by the following equation from Ref. [10].

$$Nu = 0.0331 \times Re^{0.849} \quad (18)$$

Standard $k-\omega$ has less deviation of -3.9% than SST $k-\omega$ model of -7.2% compared with the value of experimental correlation. Furthermore, a comparison of numerical and experimental results of Nusselt number distribution on the centerline of the ribbed channel for steam-only is shown in Fig. 6. It can be observed that the numerical results of pitch-averaged Nu in the fully developed region for both turbulence models are fairly consistent with experimental data at $Re = 29471$, except for the entrance region ($x/D < 1.5$), while the predicted values of pitch-averaged Nu by standard $k-\omega$ model are in better agreement with the experimental data than SST $k-\omega$ model at $Re = 58585$. This confirms the suitability of standard $k-\omega$ model in the present study. Therefore, the standard $k-\omega$ model has been employed in this study. Using therefore, not Consequently which is a word for bad outcome 你的这段和前一段讲个同一件事情，合二为一

Fig. 4. Comparison of numerical results with experimental data for area-averaged Nu varying with Re

Formatted: Indent: First line: 0 ch

Formatted: Font color: Blue

Formatted: Highlight

Formatted: Highlight

Formatted: Highlight

Formatted: Highlight

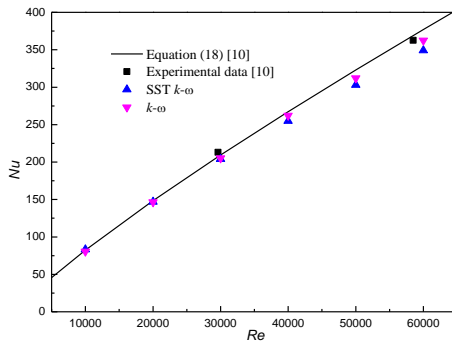


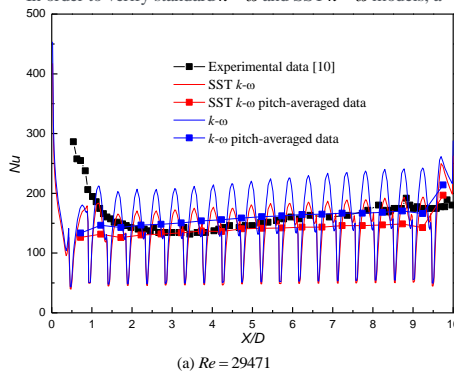
Fig. 5. Comparison of numerical results of SST and $k-\omega$ models with experimental correlation.

$k-\omega$ model have an average deviation of 6.3% at $Re=14,000$, while the deviation for SST $k-\omega$ is 14.3% under the identical conditions. Fig. 5 plots the comparison of numerical results of SST $k-\omega$ and standard $k-\omega$ models with the experimental correlation, which is given by the following equation from Ref. [10]:

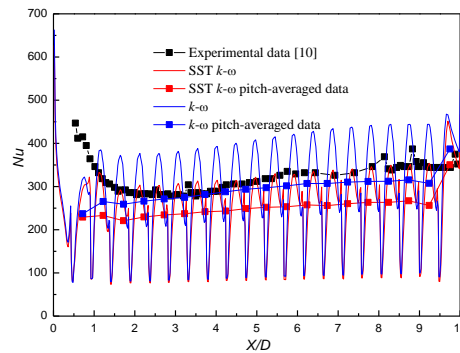
$$Nu = 0.0331 \times Re^{0.849} \quad (18)$$

It can be seen that the predicted results are in good agreement with the values of experimental correlation in the low Reynolds number range ($Re < 30,000$). However, the predicted results are also slightly lower than the value of experimental correlation, when the Reynolds number is greater than 40,000. Generally, both the standard $k-\omega$ and SST $k-\omega$ models can accurately predict this numerical simulation with the Reynolds number ranging from 10,000 to 60,000. Standard $k-\omega$ has less deviation of 3.9% than SST $k-\omega$ model of 7.2% compared with the value of experimental correlation. Consequently, the standard $k-\omega$ model has been employed in this study.

In order to verify standard $k-\omega$ and SST $k-\omega$ models, a



(a) $Re = 29471$



(b) $Re = 58585$

Fig. 6. Comparison of numerical and experimental results for centerline Nu distribution at (a) $Re = 29471$ and (b) $Re = 58585$

comparison of numerical and experimental results of Nusselt number distribution on the centerline of the ribbed channel for steam only is shown in Fig. 6. It can be observed that the numerical results of pitch-averaged Nu in fully developed region for both the two turbulence models are fairly consistent with experimental data at $Re = 29471$, except for the entrance region ($x/D < 1.5$), while the predicted values of pitch-averaged Nu by standard $k-\omega$ model are in better agreement with the experimental data than SST $k-\omega$ model at $Re = 58585$, which further confirms the accuracy of standard $k-\omega$ model adopted in the present study.

3. Results and discussion

3.1 Secondary flow distribution and its effect on heat transfer of secondary flow distribution

First of all, text must put before figure!!!, it is reversed in your result part

In order to analyze the structure and evolution of secondary flow and its effect on heat transfer in a square ribbed channel, the vortex core technology with λ_2 criterion based on ANSYS CFD POST has been employed in this study. The detailed description of the vortex core technology including vortex core identification methodology can be found in Refs. [27–28, 31]. According to Zhu et al. [27], the Reynolds number has little influence on the morphology and distribution of secondary flows in a ribbed channel, therefore, the case of Reynolds number of 60,000 has been selected in this section.

Formatted: Font color: Blue

Formatted: Font: (Asian) Chinese (PRC)

Formatted: Highlight

Formatted: Indent: First line: 0.94 ch

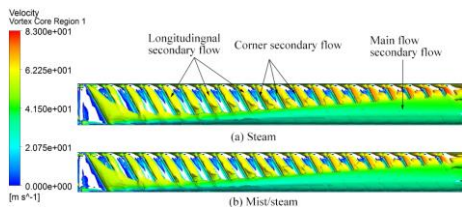


Fig. 7. Secondary flow distribution in the 60° ribbed channel with (a) steam and (b) mist/steam cooling.

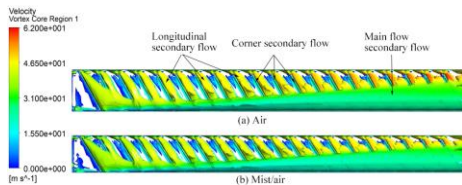


Fig. 8. Secondary flow distribution in the 60° ribbed channel with (a) air and (b) mist/air cooling.

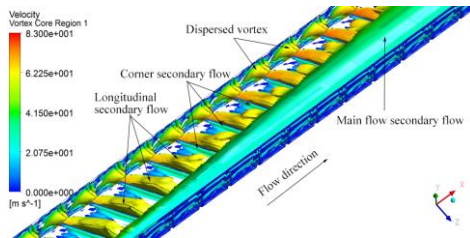


Fig. 9. The details of secondary flow distribution in fully developed region for a steam cooling ribbed channel.

POST has been employed in this study. The detailed description of the vortex core technology including vortex core identification methodology can be found in Refs. [27–28, 31]. According to Zhu et al. [27], the Reynolds number has little influence on the morphology and distribution of secondary flows in a ribbed channel, therefore, the Reynolds number of 60,000 has been selected in this section.

The morphology and distribution of secondary flows in the 60° ribbed channel with steam, mist/steam, air and mist/air are shown in Figs. 7 and 8, respectively. It is found that different coolants have insignificant influence on morphology and distribution of secondary flows. Meanwhile, the velocity contour plots I did not see the plots of these secondary flows suggest that the velocity in mist/steam cooling and mist/air cooling ribbed channel is slightly lower than that in corresponding steam cooling and air cooling channel, due to the entrainment effect of water droplets when the water droplets are suspended in the flow and transported by steam and air flow via drag [18]. However, the decrease of velocity in mist/steam and mist/air cooling channel is minimal due to a small mist mass ratio (only 2% mist) in this study.

The detailed secondary flow distribution for the steam cooling in fully developed region is depicted in Fig. 9. Move the description of the secondary flow here. The detailed secondary flow distribution in fully developed region is depicted in Fig. 9. Figs. 7 and 8 show the four coolants have insignificant influence on morphology and distribution of secondary flows. The secondary flow in the ribbed channel mainly consists of longitudinal secondary flow, main flow secondary flow, corner secondary flow, and dispersed vortex. The longitudinal secondary flow is generated at the leading edge of each rib, as a result of flow separation and development along the inclined ribs. Eventually, the longitudinal secondary flow merges into the main flow secondary flow located at the right side of the channel, which grows in size along the main flow direction. The axes of longitudinal secondary flows are consistent with the direction of inclined ribs, and the longitudinal secondary flow has three-dimensional flow characteristics with a spiral motion flowing into the downstream of the channel. Meanwhile, the main flow secondary flow has its axis in the stream-wise direction. The corner secondary flow is generated at the root of leading edge of each rib, i.e., the junction of the ribbed surface and the leading edge of inclined rib, where the local pressure is high (the local stagnation region) and develops along the inclined ribs, eventually flowing into the main flow secondary flow. The size of corner secondary flow is small, caused by the suppression of the main flow. The dispersed vortex (see Fig. 9) located at the left side of smooth wall is generated by the disturbance of the main flow when impinging the inclined ribs and dissipates in the flow field due to its destabilization.

However, the velocity contour plots of these secondary flows suggest that the velocity in mist/steam cooling and mist/air cooling ribbed channel is slightly lower than that in corresponding steam cooling and air cooling channel due to the entrainment effect of water droplets. This is because the water droplets are suspended in the flow and are transported by steam and air flow via drag [18]. The decrease of velocity in mist/steam and mist/air cooling channel is minimal due to a small mist mass ratio (only 2% mist) in this study. The secondary flow in the ribbed channel mainly consists of longitudinal secondary flow, main flow secondary flow, corner secondary flow, and dispersed vortex (see Fig. 9). The longitudinal secondary flow is generated at the leading edge of each rib, as a result of flow separation and development along the inclined ribs. Eventually, the longitudinal secondary flow merges into the main flow secondary flow located at the right side of the channel, which grows in size along the main flow direction. The axes of longitudinal secondary flows are consistent with the direction of inclined ribs, and the longitudinal secondary flow has three-dimensional flow characteristics with a spiral motion flowing into the downstream of the channel. Meanwhile, the main flow secondary flow has its axis in the stream-wise direction. The corner secondary flow is generated at the root of leading edge of each rib, i.e., the junction of the ribbed surface and the leading edge of inclined rib, where the

Formatted: Highlight

Formatted: Highlight

Formatted: Font color: Blue

Formatted: Font color: Blue

Formatted: Font: (Asian) Chinese (PRC)

local pressure is high (the local stagnation region) and develops along the inclined ribs, eventually flowing into the main flow secondary flow. The size of corner secondary flow is small, caused by the suppression of the main flow. The dispersed vortex (see Fig. 9) located at the left side of smooth wall is generated by the disturbance of the main flow when impinging the inclined ribs and dissipates in the flow field due to its destabilization.

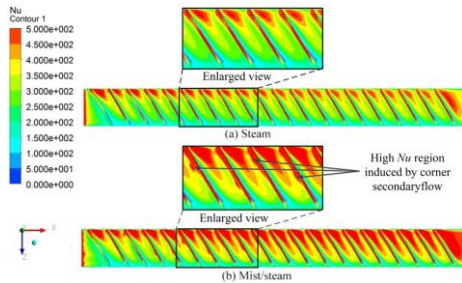


Fig. 10. Nu distribution in the ribbed channel at $Re = 60,000$ (a) steam and (b) mist/steam.

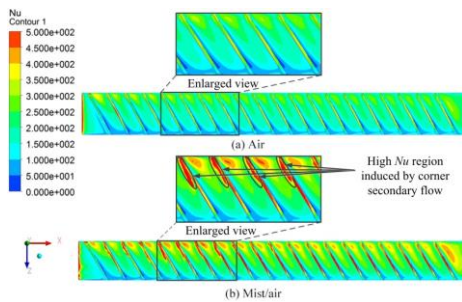
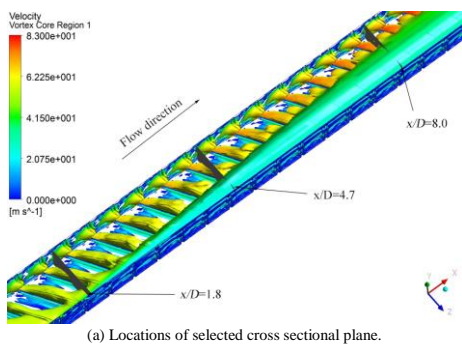
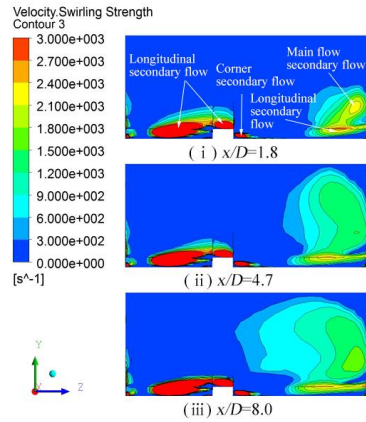


Fig. 11. Nu distribution in the ribbed channel at $Re = 60,000$ (a) air and (b) mist/air.



(a) Locations of selected cross sectional plane.



(b) Strength of longitudinal secondary flow at selected plane.

Fig. 12. The distribution of strength of longitudinal secondary flow in the flow direction

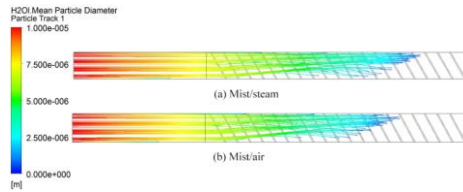


Fig. 13. The droplet trajectories at $Re = 60,000$ (a) mist/steam (b) mist/air.

The Nusselt number contour plots on ribbed surface in the 60° ribbed channel at $Re = 60,000$ for steam, mist/steam, air and mist/air cooling are shown in Figs. 10 and 11, respectively. 很明显你应该用一个图 abcd, 而不是用两个图 respectively, 你应该合并, 同理有 fig7 8. 这样, 修改起来很简单。 In general, the Nu distribution for all the cases is similar. The high Nu regions occur in the places close to the left side of smooth wall, which are covered by the longitudinal secondary flows and Nu values gradually decrease along the inclined rib direction. In addition, the Nu values are periodically distributed along the stream-wise direction for the cases of steam cooling (Fig.10 (a)) and air cooling (Fig.11 (a)). It can be clearly observed that \rightarrow . Apparently, the averaged Nu value in mist/steam cooling channel is the highest, followed by that in steam, mist/air and air cooling channel, which indicates that injecting a small amount of mist can significantly improve the heat transfer coefficient performance in the ribbed channel.

段落组织很混乱, 描述 Nu 居然放在 figure 12 之后, 明显是应该在这里, 我已经给你放在这个位置了。 As shown in the enlarged views of Figs. 10 (b) and 11(b), the enlarged

Formatted: Highlight

Formatted: Highlight

Formatted: Highlight

Formatted: Font color: Blue

Formatted: Highlight

views, the high Nu regions caused by corner secondary flow also occur at the root of leading edge of each rib for mist/steam cooling and mist/air cooling channels, but these high Nu regions are not significant in corresponding steam and air cooling channel (see Figs. 10 (a) and 11 (a)). Additionally, these high Nu regions are not noticeable along the flow direction after about the 10th rib in both the mist/steam and mist/air cooling channels. 此处分析我不同意，第十个 rib 再通道中心，和 corner 有什么特别关系？关键是图上不能显示 droplet 在哪里消失的，如果需要，你应该把 figure 13 提前。 This can be explained by the fact that the heat transfer capacity of corner secondary flow in mist/steam cooling and mist/air cooling channels is significantly enhanced due to the droplet evaporation and the droplet thermal-fluid dynamics. However, the water droplets will evaporate quickly in the process of travelling to downstream of the channel as shown in Fig. 13, which results in the additional benefits of droplet evaporation for corner secondary flow heat transfer to be reduced.

The mist cooling enhancement mechanism will be discussed in the later. 这种话不要说，说了只能证明你的结果没有很好的布局！ Mechanism of heat transfer enhancement in the ribbed channel can be interpreted by In general, the Nu distribution for all the cases is similar. The high Nu regions occur in the places close to the left side of smooth wall, which are covered by the longitudinal secondary flows and Nu values gradually decrease along the inclined rib direction. In addition, the Nu values are periodically distributed along the stream-wise direction for the cases of steam cooling (Fig.10 (a)) and air cooling (Fig.11 (a)). The secondary flow heat transfer enhancement mechanism can be interpreted as follows: evolution. On the one hand, mass transfer between the boundary region and main flow increases temperature gradient to enhance the heat transfer effectively. The down-wash on one side of longitudinal secondary flow can take bring the main flow with high momentum and low temperature into the boundary layer, where strong momentum and energy exchange take place, tense not right happens, since the increasing temperature gradient can enhance the heat transfer effectively. In the meantime, the up-wash on the other side of longitudinal secondary flow pushes the fluid in the boundary layer with high temperature and low momentum into the main flow region and exchange momentum and energy with mainstream again. On the other hand, the secondary flow between ribs destroy the stable boundary flow found in the smooth channel. As analyzed previously, the longitudinal secondary flow has three-dimensional characteristics in a manner of spiral flow lasting over a long distance along the downstream of the channel, which can continuously destroy the boundary layer downstream of the channel resulting in significantly enhancing the local heat transfer rate.

According to Gentry et al. [33], the strength of secondary flow and the location of secondary flow core relative to boundary layer are the two key factors influencing on heat transfer characteristics, i.e., the stronger strength of secondary

flow and the closer distance between the secondary flow core and boundary layer will obtain the higher heat transfer. Fig. 12 shows the strength distribution of longitudinal secondary flow at selected positions along the stream-wise direction, where the selected locations are shown in Fig. 12 (a). It can be seen from Fig. 12 (b) that the strength distribution of longitudinal secondary flow along the stream-wise direction is similar, which results in the Nu values to be periodically distributed in the same direction for the cases of steam and air cooling channel (see Figs. 10 (a) and 11 (a)), whereas the strength of longitudinal secondary flows along the transverse direction gradually decreases, which leads to leading to the decreasing Nu values also decreasing in the same longitudinal or streamwise direction for all the cases. It should be noted that the size of the main flow secondary flow becomes larger and larger and its strength is weakened (I can not find evidence from your figure), in contrast with the constancy of longitudinal secondary flow along main flow direction. Furthermore, a large distance between the main flow secondary flow core to the ribbed surface is existed, which results in the contribution of main flow secondary flow to heat transfer to be limited for the cases of steam cooling and air cooling. However, the main flow secondary flow may contribute to the heat transfer in mist/steam cooling and mist/air cooling channels. As shown in Figs. 10 (b) and 11 (b), the Nu values along the stream-wise direction gradually increases, which may be caused by the interaction between the main flow secondary flow and water droplets. Fig. 13 shows the water droplet trajectories colored by the droplet mean diameter at $Re = 60,000$ in mist/steam and mist/air cooling channels. It can be observed that the trajectories of droplets are greatly affected by the main flow secondary flow. The droplets close to the right side of smooth wall are in the form of spiral flow travelling to downstream of the channel due to the entrainment of main flow secondary flow, followed by quick droplets evaporation and enhanced local heat transfer rate.

As shown in Figs. 10 (b) and 11 (b), the enlarged views, the high Nu regions caused by corner secondary flow also occur at the root of leading edge of each rib for mist/steam cooling and mist/air cooling channels, but these high Nu regions are not significant in corresponding steam and air cooling channel (see Figs. 10 (a) and 11 (a)). Additionally, these high Nu regions are not noticeable along the flow direction after about the 10th rib in both the mist/steam and mist/air cooling channels. This can be explained by the fact that the heat transfer capacity of corner secondary flow in mist/steam cooling and mist/air cooling channels is significantly enhanced due to the droplet evaporation and the droplet thermal-fluid dynamics. However, the water droplets will evaporate quickly in the process of travelling to downstream of the channel as shown in Fig. 13, which results in the additional benefits of droplet evaporation for corner secondary flow heat transfer to be reduced.

3.2 Effect of Reynolds number on heat transfer

Formatted: Highlight

Formatted: Highlight

Formatted: Highlight

Formatted: Highlight

Formatted: Highlight

Formatted: Highlight

Formatted: Highlight

Formatted: Highlight

Formatted: Highlight

Formatted: Highlight

Formatted: Font color: Blue

Formatted: Highlight

Formatted: Highlight

Formatted: Font color: Blue

In order to analyze the influence of Reynolds number on heat transfer characteristics of the four coolants, the inlet temperature and pressure in this section are specified as 160°C and 0.1MPa. Fig. 14 illustrates the area-averaged Nu of the ribbed surface in the ribbed channel for the four coolants varying with Reynolds number from 10000 to 60000. In order to analyze the influence of Reynolds number on heat transfer characteristics of the four coolants, the inlet temperature and pressure in this section are specified as 160°C and 0.1MPa. It can be observed that the averaged Nu for each all the coolants increases with the increase of Reynolds number and the averaged Nu of mist/steam cooling obtains the highest averaged Nu , followed by that of steam, mist/air and air cooling. The heat transfer enhancement of mist/steam cooling as compared to steam cooling is relatively small when for Reynolds number is less than 30,000, while that cooling performance is significantly improved when Reynolds number is greater than 40,000. The heat transfer enhancement of mist/air cooling compared with air cooling raises slightly with Reynolds number. For example, the heat transfer enhancement of mist/steam cooling and mist/air cooling is 17.87% and 37.62% at $Re = 30,000$, in contrast with 72.13% and 44.57% at $Re = 60,000$. Under the condition of $Re = 60,000$, the averaged Nu of mist/steam, steam, and mist/air cooling boosts by about 200%, 74.29% and 44.57% as compared to that of air cooling.

The thermal performance factor for the four kinds of coolants varying with Reynolds number is shown in Fig. 15. It can be concluded that the mist/steam cooling achieves the best thermal performance, followed by that of steam, mist/air and air cooling. Note that, a similar thermal performance can be observed for steam cooling and mist/air cooling. Furthermore, the thermal performance of mist/steam cooling greatly increases with Re -Reynolds number (一句话里面不要用两次 increase) increases, whereas that of steam, mist/air and air cooling is slightly reduced with the increasing of Reynolds number. In general, over all the Reynolds numbers (all Re 这种话千万别说!) For the tested Reynolds numbers in this study, the heat transfer thermal performance of mist/steam, steam and mist/air cooling is enhanced by 130.9%, 62.95% and 63.29% as compared to air cooling.

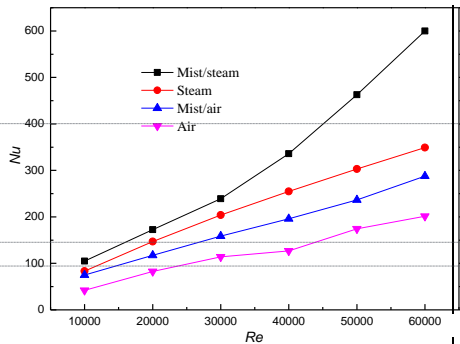


Fig. 14. The averaged Nusselt number variation for the four coolants with Reynolds number

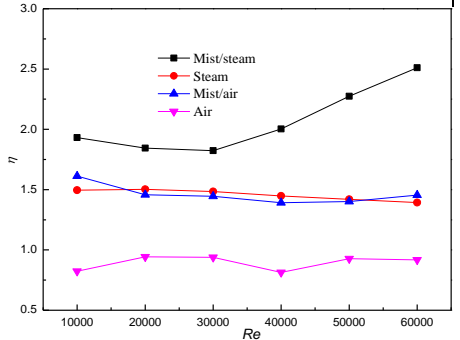
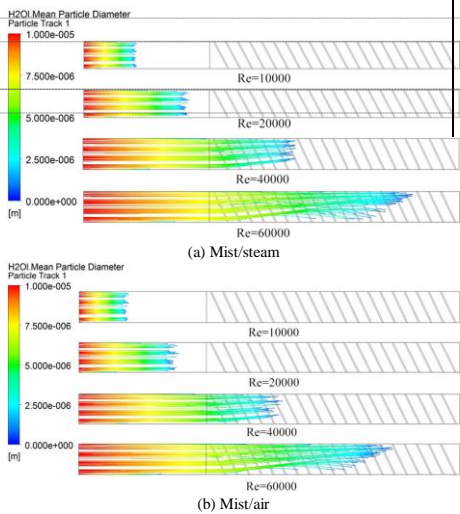


Fig. 15. The thermal performance factor variation for the four coolants with Reynolds number



Formatted: Font color: Blue

Formatted: Font color: Blue

Formatted: Font color: Blue

Formatted: Highlight

Formatted: Highlight

Formatted: Highlight

Formatted: Highlight

Formatted: Font color: Blue

Fig. 16. The droplet diameter variation with Reynolds number for (a) mist/steam (b) mist/air

According to Guo et al. [14, 15], the heat transfer enhancement of mist/steam cooling is caused by the following factors: (a) Due to the latent heat of evaporation, the mean bulk temperature of the steam flow greatly decreases and a steep temperature gradient near the boundary layer is obtained. (b) The steam mass flow rate progressively increases due to the added steam mass from droplets evaporation inside the steam flow. (c) Due to the droplets evaporation, the momentum, heat and mass transfer between the droplets and the steam flow increase the turbulence mixing and accelerate the heat circulation, which results in increasing the heat transfer rate of mist/steam flow. Fig. 16 illustrates the trajectories of water droplets colored by particle diameter with different Reynolds numbers for mist/steam and mist/air cooling. It can be seen that the droplets have completely evaporated before entering into the heated section in the lower Reynolds number range ($Re < 20,000$) for both the cases of mist/steam and mist/air cooling, which means that the benefits of additional turbulence mixing induced by interaction between water droplets and steam or air flow and droplets thermal-fluid dynamics are greatly diminished. On the other hand, the added steam mass flow rate due to the droplet evaporation is weak because the mass ratio of water droplets over steam flow is very small (2% mist) considered in this study. As a result, the heat transfer enhancement of mist/steam and mist/air under the condition of $Re < 20,000$ is only determined by the single-phase flow convection and a lower bulk temperature due to the droplet evaporation. This is the reason why the heat transfer enhancement of mist/steam and mist/air is limited in the lower Reynolds number range. When the Reynolds number is greater than 40,000, a large number of droplets can be entrained into the heated section, where the trajectories of droplets are greatly affected by the secondary flows in ribbed channel. In addition to an increased steam or air mass flow rate and higher latent heat of evaporation caused by the raised Reynolds number. The turbulence mixing in heated section is also increased due to the interaction between the secondary flows and droplets as well as droplet thermal-fluid dynamics, which contributes to improving the heat transfer rate. This could be the reason why the heat transfer enhancement of mist/steam is significantly increased when Reynolds number exceeds 40,000.

Except for the aforementioned factors, the heat transfer enhancement of mist/steam can be also attributed to the following aspects: Firstly, under the current operating conditions, the specific heat capacity of steam coolant is 1.9 times higher than that of air, whereas the thermal conductivity of steam is approximately 0.83 times lower than that of air, resulting in the heat transfer capacity of steam is better than that of air. It implies that the heat transfer capacity of mist/steam is still better than that of mist/air when injecting the same amount of mist into corresponding coolant flow. Secondly, the density of steam is about 0.63 times lower than that of air,

which results in the velocity of mist/steam is higher than that of mist/air with the same mass flow rate [22]. Finally, mist/steam is essentially distinct from mist/air. The mist/steam cooling is one-component two-phase flow, where the evaporation process of mist is determined by the pressure of steam flow; the mist/air cooling is two-component two-phase flow, where the evaporation process of mist is controlled by the partial pressure of water vapor, not by total pressure of the mixture [14]. It means that the rate of droplet evaporation in mist/air cooling is higher than that in mist/steam cooling as shown in Fig. 16, which also decreases the heat transfer rate of mist/air. 此处我不确定没读过相关文献，你可以考虑此处加引用。 It should be noted that the heat transfer capacity of steam is better than that of mist/air in our simulations. This could be attributed to the fact that the mist mass ratio over air flow is small (only 2%) in this study. As discussed above, the heat transfer capacity of mist/steam is the highest, followed by steam, mist/air and air, which is also consistent with the result in Refs. [22–24]. 最近一句放在此处好像不是很合适。

3.3 Effect of pressure on heat transfer

To investigate the effect of pressure on heat transfer characteristics of the four coolants, Reynolds number and inlet temperature are fixed as 30,000 and 160°C in this section. Figs. 17 and 18 plot the effect of pressure ranging from 0.1Mpa to 0.5MPa on the averaged Nu and the thermal performance factor for the four coolants. Reynolds number and inlet temperature are fixed as 30,000 and 160°C in this section, to investigate the effect of pressure on heat transfer characteristics of the four coolants. It can be concluded that the pressure seems to have limited influence on heat transfer for three coolants except for the case of mist/air cooling, i.e., no significant changes in the averaged Nu and the thermal performance factor for the cases of mist/steam, steam and air cooling can be observed within the range of pressure. However, the averaged Nu and the thermal performance factor for mist/air cooling drop by about 18.7% and 15.08%, respectively, for the pressure ranging from 0.1Mpa to 0.5MPa. It should be noted that the averaged Nu and thermal performance of mist/steam cooling are still the highest among all the coolants, followed by those of steam, mist/air and air cooling.

For the cases of single-phase (steam-only and air-only) flow convective heat transfer, the Prandtl number (Pr) increases by 6.2% for steam cooling and remains constant for air cooling for pressure ranging from 0.1Mpa to 0.5MPa. It suggests that the effect of pressure on heat transfer for steam and air cooling can be neglected. This result is consistent with that of Ref. [10]. For the cases of two-phase (mist/steam and mist/air) flow, the evaporation process of droplets is sensitive more easily affected to by operating conditions including pressure and temperature. Fig. 19 depicts the droplet diameter varying with pressure for mist/steam cooling and mist/air cooling at $Re = 30,000$. It can be observed that the travelling distance of water droplets is greatly reduced as the pressure increases

Formatted: Highlight

Formatted: Font color: Blue

Formatted: Highlight

for both the cases. When the pressure is greater than 0.3MPa, the water droplets can not survive at the inlet of the heated section, which means that the heat transfer in such a case is mainly determined by the single-phase flow convection and a lower bulk temperature due to the droplet evaporation, resulting in the averaged Nu of mist/steam cooling nearly remaining immutable. For the case of mist/air cooling, which is thermodynamically different

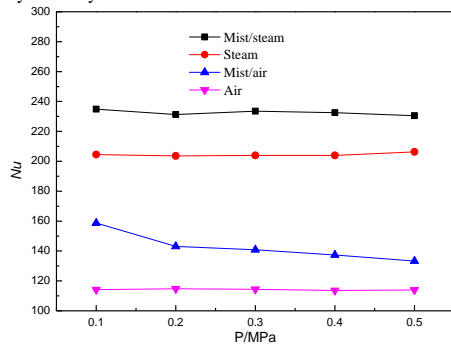


Fig. 17. The averaged Nusselt number variation for the four coolants with pressure at $Re = 30,000$

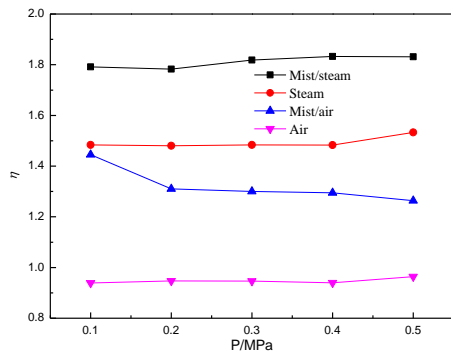


Fig. 18. The thermal performance factor variation for the four coolants with pressure at $Re = 30,000$

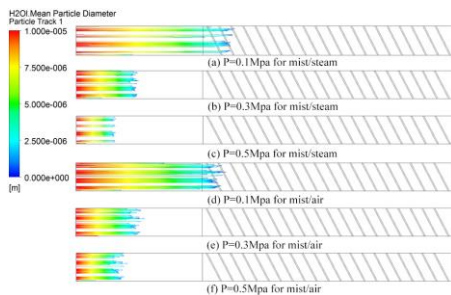


Fig. 19. The droplet diameter variation with pressure for mist/steam and mist/air cooling at $Re = 30,000$

from mist/steam cooling as analyzed in section 3.2, the water droplets for mist/air cooling are more susceptible to pressure and evaporate quickly with the increase of pressure as compared to mist/steam cooling. Additionally, the mist ratio considered in this study is small (2%), thus the water droplet evaporation has limited contribution to the thermal property of gas flow such as the specific heat and Prandtl number. As discussed above, increasing the pressure will decrease the heat transfer capacity of mist/air cooling.

3.4 Effect of temperature on heat transfer

The effect of inlet temperature ranging from 120°C to 200°C on heat transfer characteristics for the four coolants is analyzed in this section with a constant pressure of 0.1MPa and Reynolds number of 30,000. Fig. 20 shows the averaged Nu varying with temperature for different coolants. It can be seen that the averaged Nu drops as the temperature increases for all coolants, while the decrease of averaged Nu for mist/steam and mist/air cooling over the investigated temperature range is more significant than that of corresponding steam and air cooling cases. When the temperature increases from 120°C to 200°C, the averaged Nu of mist/steam and mist/air cooling decreases by 31.13% and 29.24%, whereas that of steam and air cooling drops by 16.08% and 12.83%, respectively. In addition, the heat transfer enhancement of mist/steam and mist/air cooling compared with corresponding steam and air cooling also drops from 39.03% to 14.09% and from 49.18% to 21.09%, respectively, for the temperature ranging from 120°C to 200°C. It is confirmed that increasing temperature will greatly reduce the heat transfer enhancement of two-phase flow.

The thermal performance factor of the four coolants varying with temperature is depicted in Fig. 21. The thermal performance of mist/steam, steam, mist/air and air cooling also decreases by 31.57%, 15.53%, 30.36% and 11.3%, respectively, as the temperature rises from 120°C to 200°C. It means that the thermal performance of mist/steam and mist/air cooling is significantly reduced by the increase of temperature as compared to corresponding steam and air cooling. Note that, the averaged Nu and the heat transfer performance of mist/steam cooling is also the highest, followed by that of steam, mist/air and air cooling as observed in Figs. 20 and 21.

The trajectories of water droplets colored by particle diameter varying with the temperature for both mist/steam and mist/air cooling are illustrated in Fig. 22. The decreased traveling distance of water droplets is observed with the increase of temperature for both the cases. Since higher temperature results in a higher rate of evaporation when the temperature is above the droplet boiling point (see Eq. (9)). When the temperature reaches 200°C, the droplets can not survive at the

Formatted: Highlight

Formatted: Highlight

Formatted: Highlight

Formatted: Highlight

Formatted: Highlight

Formatted: Font color: Blue

inlet of the heated section, leading to the worse heat transfer for two-phase flow as analyzed previously. It must be noted that the averaged Nu of steam and air cooling also decreases with the rising of temperature, which is in accordance with the result of Ref. [11] with maximum decrease of 10% for the temperature of steam ranges from 300°C to 500°C. However, it is inconsistent with the result of Ref. [10], where the superheat of steam coolant has insignificant influence on its heat transfer coefficient. This can be explained that the superheat range of steam (from 20°C to 80°C) adopted in this study is higher than that adopted in Ref. [10] (from 13°C to 51°C).

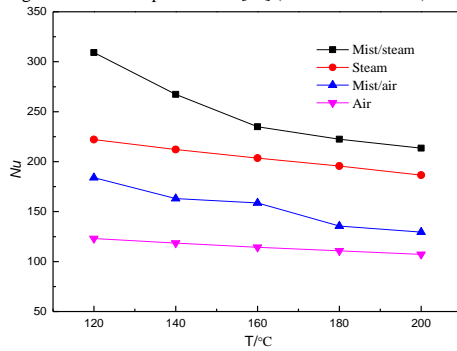


Fig. 20. The averaged Nusselt number variation for the four coolants with temperature $Re = 30,000$

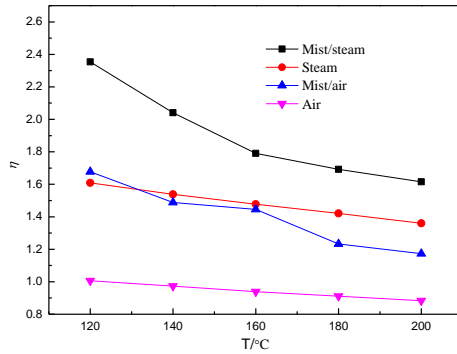


Fig. 21. The thermal performance factor variation for the four coolants with temperature $Re = 30,000$

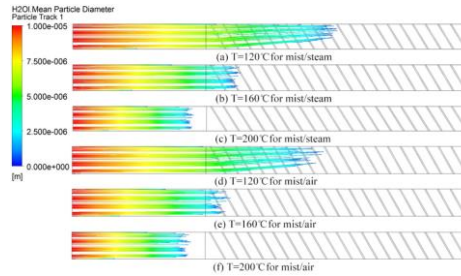


Fig. 22. The droplet diameter variation with temperature for mist/steam and mist/air cooling at $Re = 30,000$

Theoretically, increasing the temperature of coolant will diminish the temperature difference between the fluid and the heated surface, which results in decreasing the heat transfer capacity of coolant. 此处和实验不一致的解释一定要小心，想温度身高，比热容是不是下降了？等等，或许可以解释。

4. Conclusions

In this numerical study, morphology and distribution of secondary flow and its effects on Nu in 60° ribbed channel are investigated. The effect of operating conditions including Reynolds number, pressure and temperature on the flow and heat transfer characteristics of two-phase flow and single-phase flow has been analyzed in detail. A comparison of heat transfer characteristics between two-phase flow mist cooling and single-phase flow steam and air cooling has been conducted under the same operating conditions. Turbulence model validation performed in this study shows that the predicted values of standard $k-\omega$ model agree well with experimental data. The conclusions are drawn below:

(1) The droplets have insignificant impact on the morphology and distribution of secondary flow in the ribbed channel, but the trajectories of droplets are greatly affected by the secondary flow. The high Nu regions covered by longitudinal secondary flows have periodically distributed Nu value along the stream-wise direction and gradually decrease along the transverse direction for the case of single-phase flow, which is caused by the strength of longitudinal secondary flow being similar along the stream-wise direction and progressively decreasing along the transverse direction. For the case of two-phase flow, the Nu values gradually increase along the stream-wise direction due to the interaction between the main flow secondary flow and water droplets.

(2) When the Reynolds number is less than 20,000, the water droplets can not survive at the inlet of the heated section, where the heat transfer enhancement of mist/steam and mist/air cooling is only determined by single-phase flow convection and a lower bulk temperature due to the droplet evaporation; under the operating condition of $Re > 40,000$, plenty of droplets can be entrained into the heated section, where the heat transfer enhancement of mist/steam and mist/air cool-

ing is largely decided by an increased mass flow rate, higher latent heat of evaporation and an increased turbulence mixing due to the gas-droplet interactions and droplets thermal-fluid dynamics.

(3) The averaged Nu for the four coolants increases as Reynolds number increases. The averaged Nu of mist/steam, steam, and mist/air cooling rises by about 200%, 74.29% and 44.57% compared with that of air cooling at $Re = 60,000$, respectively. The thermal performance of mist/steam cooling increases as Reynolds number increases, in contrast with the other three coolants. Over the test range of Reynolds number, the heat transfer thermal performance of mist/steam, steam and mist/air cooling boosts by 130.9%, 62.95% and 63.29%, respectively, as compared to air cooling.

(4) The pressure has no evident impact on heat transfer of mist/steam, steam and air within the range of pressure tested in this study, because the change of Prandtl number under this situation for the cases of steam and air is minimal. However, the averaged Nu and thermal performance for the case of mist/air drop by about 18.7% and 15.08%, respectively, with the pressure ranging from 0.1MPa to 0.5MPa. It could be interpreted by the fact that the rate of droplet evaporation of mist/air is more susceptible to pressure, resulting in the droplets evaporating more quickly.

(5) The temperature has a greater impact on heat transfer of two-phase flow than that of single-phase flow. When the temperature increases from 120°C to 200°C, the averaged Nu of mist/steam and mist/air cooling is reduced by 31.13% and 29.24%, whereas that of steam and air cooling is decreased by 16.08% and 12.83%; the thermal performance factor of mist/steam and mist/air cooling is reduced by 31.57% and 30.36%, whereas that of steam and air cooling drops only by 15.53% and 11.3%. It implies that increasing temperature will significantly decays the heat transfer performance of two-phase flow mist cooling.

Acknowledgment

This work is financially supported by the National Natural Science Foundation of China (No.50806059) and the Innovative Research Team in University of Ministry of Education of China (IRT1280).

Nomenclature

D	: Hydraulic diameter of channel, mm.
e	: Rib eight, mm.
f	: Dimensionless friction coefficient.
f_o	: Friction coefficient for fully developed region in a smooth tube.
H	: Height of channel, mm.
ΔL	: Length of channel, mm.
L_e	: Extended entrance section, mm.
L_h	: Length of heated section, mm.
L_o	: Extended outlet section, mm.
Nu	: Nusselt number.

Nu_o	: Nusselt number for fully developed region in a smooth tube.
p	: Rib pitch, mm.
P	: Static pressure
ΔP	: Pressure loss of channel, Pa.
Pr	: Prandtl number.
q	: Heat flux, W/m ² .
Re	: Reynolds number.
T_w	: Temperature of the ribbed side wall, K.
T_b	: bulk temperature at x-direction, K.
u	: Inlet velocity of channel, m/s.
W	: Width of channel, mm.
μ	: Fluid dynamic viscosity, m ² /s.
α	: Rib angle, °.
λ	: Thermal conductivity, W m ⁻¹ K ⁻¹ .
η	: Thermal performance factor.

References

- [1] J. C. Han and J. S. Park, Developing heat transfer in rectangular channels with rib turbulators, *International Journal of Heat and Mass Transfer*, 31 (1) (1988) 183-195.
- [2] J. C. Han, S. Ou, J. S. Park and C. K. Lei, Augmented heat transfer in rectangular channels of narrow aspect ratios with rib turbulators, *International Journal of Heat and Mass Transfer*, 32 (9) (1989) 1619-1630.
- [3] J. C. Han, Heat transfer and friction characteristics in rectangular channels with rib turbulators, *Journal of Heat Transfer*, 110 (2) (1988) 321-328.
- [4] J. S. Park, J. C. Han, Y. Huang, S. Ou, and R. J. Boyle, Heat transfer performance comparisons of five different rectangular channels with parallel angled ribs, *International Journal of Heat and Mass Transfer*, 35 (11) (1992) 2891-2903.
- [5] J. Y. Gong, T. Y. Gao and G. J. Li, Contrastive experimental study on heat transfer and friction characteristics in steam cooled and air cooled rectangular channels with rib turbulators, *Journal of Mechanical Science and Technology*, 28 (9) (2014) 3845-3854.
- [6] J. Y. Gong, T. Y. Gao and G. J. Li, Heat transfer and friction characteristics in steam cooled rectangular channels with rib turbulators, *Journal of Mechanical Science and Technology*, 28(1) (2014) 357-364.
- [7] J. Z. Liu, J. M. Gao and T. Y. Gao, An experimental investigation of heat transfer characteristics in a steam-cooled square channel with rib turbulators, *ASME paper No. GT2011-46134*.
- [8] J. Z. Liu, J. M. Gao, T. Y. Gao and X. J. Shi, Heat transfer characteristics in steam-cooled rectangular channels with two opposite rib-roughened walls, *Applied Thermal Engineering*, 50 (1) (2013) 104-111.
- [9] X. J. Shi, J. M. Gao, L. Xu and F. J. Li, Heat transfer performance comparison of steam and air in gas turbine cooling channels with different rib angles, *Heat and Mass Transfer*, 49 (11) (2013) 1577-1586.
- [10] J. Z. Liu, J. M. Gao and T. Y. Gao, Forced convection heat transfer of steam in a square ribbed channel, *Journal of Me-*

- chanical Science and Technology, 26 (4) (2012) 1291-1298.
- [11] L. Q. Shui, J. M. Gao, X. J. Shi, J. Z. Liu and L. Xu, The effect of cooling conditions on convective heat transfer and flow in a steam-cooled ribbed duct, *Journal of Mechanical Science and Technology*, 28 (1) (2014) 331-341.
- [12] D. W. Mukavetz, R. Wenglarz, N. Nirmalan and T. Daehler, Advanced Turbine System ATS Turbine Modification for Coal and Biomass Fuels, *Proceedings of the Advanced Turbine System Annual Program Review Meeting*, (1994) 9-11.
- [13] D. Mukherjee, Combined gas turbine and steam turbine power station, *U.S. Patent No.4424668* (1984).
- [14] T. Guo, T. Wang and J. L. Gaddis, Mist/Steam Cooling in a Heated Horizontal Tube—Part 1: Experimental System, *Journal of turbomachinery*, 122 (2) (2000) 360-365.
- [15] T. Guo, T. Wang and J. L. Gaddis, Mist/Steam Cooling in a Heated Horizontal Tube—Part 2: Results and Modeling, *Journal of turbomachinery*, 122 (2) (2000) 366-374.
- [16] T. Guo, T. Wang and J. L. Gaddis, Mist/steam cooling in a 180-degree tube bend, *Journal of heat transfer*, 122(4) (2000) 749-756.
- [17] R. Ragab and T. Wang, An investigation of applicability of transporting water mist for cooling turbine vanes, *ASME Paper No.GT2012-70110*.
- [18] T. Wang and R. Ragab, Investigation of Applicability of Transporting Water Mist for Cooling Turbine Blades, *ASME Paper No.GT2014-25818*.
- [19] T. S. Dhanasekaran and T. Wang, Validation of mist/steam cooling CFD model in a horizontal tube, *ASME Heat Transfer Summer Conference collocated with the Fluids Engineering, Energy Sustainability, and 3rd Energy Nanotechnology Conferences*. ASME, (2008) 611-624.
- [20] T. S. Dhanasekaran and T. Wang, Numerical model validation and prediction of mist/steam cooling in a 180-degree bend tube, *International Journal of Heat and Mass Transfer*, 55 (13) (2012) 3818-3828.
- [21] T. S. Dhanasekaran and T. Wang, Computational analysis of mist/air cooling in a two-pass rectangular rotating channel with 45-deg angled rib turbulators, *International Journal of Heat and Mass Transfer*, 61 (2013) 554-564.
- [22] F. N. Elwekeel, Q. Zheng and A. M. Abdala, Heat Transfer and Flow Characteristics in 90-deg Ribbed Duct Using Different Coolants, *ASME Paper No.GT2013-94908*.
- [23] G. L. Liao, X. J. Wang, J. Li and F. Zhang, A numerical comparison of thermal performance of in-line pin-fins in a wedge duct with three kinds of coolant, *International Journal of Heat and Mass Transfer*, 77 (2014) 1033-1042.
- [24] F. Zhang, X. J. Wang, J. Li. Effects of coolants on the flow and heat transfer characteristics in a non-rotating and rotating two-pass rectangular channel. *International Journal of Heat and Mass Transfer*, 91(2015) 390-400.
- [25] F. N. Elwekeel, Q. Zheng and A. M. Abdala, Numerical Study of Turbulent Flow Through Rib-Roughened Channels With Mist Injection, *ASME Paper No.GT2014-25408*.
- [26] F. N. Elwekeel, Q. Zheng and A. M. Abdala, Air/mist cooling in a rectangular duct with varying shapes of ribs, *Proceedings of the Institution of Mechanical Engineers, Part C: Journal of Mechanical Engineering Science*, 2013: 0954406213512295.
- [27] J. N. Zhu, T. Y. Gao, J. Li, G. J. Li and J. Y. Gong, The Effect of Vortex Core Distribution on Heat Transfer in Steam Cooling of Gas Turbine Blade Internal Ribbed Channels, *ASME Paper No.GT2014-25324*.
- [28] J. N. Zhu, T. Y. Gao, J. Li, G. J. Li and J. Y. Gong, Numerical Investigation of Secondary Flow Vortex Core Structure in the Two-Pass Rectangular Channel With 45° Ribs, *ASME Paper No.GT2015-42782*.
- [29] A. Durmuş, A. Durmuş, and M. Esen, Investigation of heat transfer and pressure drop in a concentric heat exchanger with snail entrance, *Applied Thermal Engineering*, 22 (3) (2002): 321-332.
- [30] F. Ozgen, M. Esen, and H. Esen, Experimental investigation of thermal performance of a double-flow solar air heater having aluminium cans, *Renewable Energy*, 34(11) (2009): 2391-2398.
- [31] T. Y. Gao, J. N. Zhu, C. W. Liu and J. M. Xu, Numerical study of conjugate heat transfer of steam and air in high aspect ratio rectangular ribbed cooling channel, *Journal of Mechanical Science and Technology*, 30(3) (2016) 1431-1442.
- [32] ANSYS Release 14.0 Help Document. ANSYS, Inc., USA, 2012.
- [33] M. C. Gentry and A. M. Jacobi, Heat transfer enhancement by delta-wing vortex generators on a flat plate: Vortex interactions with the boundary layer, *Experimental Thermal and Fluid Science*, 14 (3) (1997) 231-24.



Tiejun Gao: First author, Ph.D. Born in 1973, China. Currently works in Xi'an Jiaotong University. His major research includes two-phase flow in turbomachinery and the air and steam cooling technology of gas turbine.